physica status solidi b
www.pss-b.com
basic solid state physics

Part of Special Issue on Semiconductor Spintronics

The rise of spin noise spectroscopy in semiconductors: From acoustic to GHz frequencies

Feature Article

**Jens Hübner*, Fabian Berski, Ramin Dahbashi, and Michael Oestreich**

Institute for Solid State Physics, Leibniz Universität Hannover, Appelstr. 2, 30167 Hannover, Germany

* Corresponding author: e-mail jhuebner@nano.uni-hannover.de, Phone: +49 511 762 2903, Fax: +49 511 762 2904

This article gives an overview on the advance of spin noise spectroscopy (SNS) in semiconductors in the past 8 years from the first measurements in bulk n-GaAs [Oestreich et al., Phys. Rev. Lett. **95**, 216603 (2005)] up to the recent achievement of optical detection of the intrinsic spin fluctuations of a single hole confined in an individual self-assembled quantum dot [Dahbashi et al., arXiv:1306.3183 (2013)]. We discuss the general technical implementation of optical SNS and the invaluable profit of the introduction of real-time fast Fourier transform analysis into the data acquisition. By now, the full spin dynamic from the milli- to picosecond timescales can be addressed by SNS and the technique quickly strides ahead to enable real quantum non-demolition measurements in semiconductors.
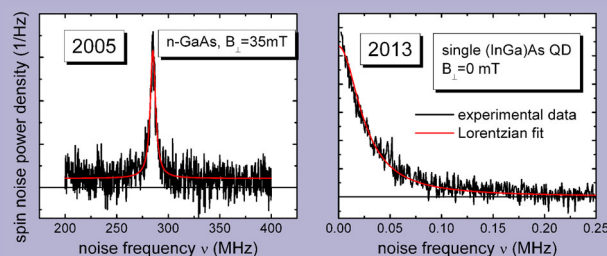
Spin noise spectra recorded in 2005 in bulk n-GaAs with approximately 10^9 electron spins (Oestreich et al.) and 2013 (Dahbashi et al.) for a single hole spin. The integration time for the latter is more than a factor of 40 shorter due to the significant advances in the measurement technique.

1 Introduction The extraction of useful information from seemingly completely incoherent processes has been a unique field in the applied and theoretical sciences ever since. Such processes do not only appear in distinct systems like the Brownian motion of microscopic entities [3, 4], zero point fluctuations in quantum mechanics [5], or the light emission of thermal radiation sources [6, 7] but are also present in such large scale systems as weather, traffic, and nowadays information flow. The linking discipline of all of these fields is statistical physics whereas the ever-present fundamental thermodynamical fluctuations become apparent as the ubiquitous phenomenon of noise. In general, noise is not always an obstacle, which makes exact measurements difficult in experimental physics, but in contrast contains all information about the dynamical properties on how a system would return back to equilibrium if it had been excited before. The closed mathematical description of this fundamental connection between noise and the temporal relaxation dynamic is given by the fluctuation–dissipation theorem [8].

The change of a distinct initial, i.e., prepared, state due to relaxation and dephasing processes plays a major role as well in all systems, which deal with the quantum mechanical entity of the spin. The spin degree of freedom in solid state systems, especially in semiconductors, has attracted a great attention over the past decade in the field of semiconductor spintronics [9–11]. The main focus in this research field comprises the exploitation and targeted control and manipulation of the carrier and nuclear spin in order to establish information processing techniques, which do not only rely on the charge of carriers. A vast number of experimental methods already exist, which are capable to extract information on the spin dynamic in a large range of semiconductor systems [12]. Among the optical methods

Wiley Online Library

Feature
_____
Article

Phys. Status Solidi B 251, No. 9 (2014)   1825

spin noise spectroscopy (SNS) matured over the past 8 years (cf. Refs. [1, 2]) into a very powerful and versatile tool with distinct advantages for the investigation of the spin dynamic in a variety of semiconductor systems [13, 14].

The first part of this article briefly reviews the basic concepts of SNS followed by the presentation of the state of the art along with the achievement of specific milestones in SNS. The last section provides an outlook how SNS might develop in the near future.

2 Basics of spin noise It was already Felix Bloch who noted in his famous paper about nuclear induction in 1946 [15] that even in the absence of any orientation by an external magnetic field one can expect in a sample with N nuclei of magnetic moment μ to find a resultant moment of the order $N^{1/2} \cdot \mu$ because of the statistically incomplete cancellation for any given projection axis. For such non-interacting spins – which applies in the most general case as well to the independent spins of atoms in gases or of electrons or holes in semiconductors – the sample system does not bear a permanent polarization of the spins. The present spin polarization is purely stochastic and its decay or rising dynamic is characterized by the specific spin coherence or relaxation time τ_s. The effects determining τ_s and leading for instance to decoherence are manifold and very strongly depend upon the system under investigation. A pure quantum mechanical treatment of homogenous quantum-decoherence is possible [16–18] but most often the representation of a random walk on the Bloch sphere is easier expressible with a characteristic correlation time picturing homogeneous and inhomogeneous dephasing processes depending on the type of correlation [19].

2.1 Measurement of spin noise Noise spectroscopy in general relies upon the fact that the complete temporal dynamic of a system at thermal equilibrium can be gathered from the noise spectrum of the investigated entity _without_ driving the system out of equilibrium [8]. There are several ways of detecting the noise of fluctuating spins. First successful approaches are based upon nuclear magnetic resonance techniques [20]. Others followed using magneto-metric methods [21–23]. Rugar and coworkers [24–29] have chosen an elegant method to extract the magnetic dissipation and fluctuations by magnetic force microscopy. However, in all systems, which have sufficient spin and orbital degrees of freedom and accessible optical transitions – which holds for most atoms and semiconductor alloys – the spin dynamic can as well be probed optically due to the optical selection rules [30, 31]. Hence, an effective but fluctuating spin polarization can be mapped onto the intensity of a transmitted probe light beam due to dichroic bleaching of the participating optical transitions [32–34]. However, any continuous or modulated injection of carriers due to absorption can alter the spin dynamic significantly. Especially in semiconductors optical pumping induces spin dephasing mechanisms, which often overshadow the inherent spin dynamic [35–37]. A widely employed

alternative to investigate the spin dynamic without the obstacles of optical pumping is optical Faraday rotation with probe photon energies in the transparent regime. In the field of semiconductor physics, this holds for photon energies below the band gap.

In optical SNS, the effective spin polarization at thermal equilibrium gives rise to Faraday rotation of the transmitted linear light polarization. The two circular light components, which represent the linear light polarization, experience different dispersions in the sample due to the optical spin selection rules. The first successful optical measurement of spin noise by Faraday rotation in the transparent regime was achieved by Aleksandrov and Zapasskii [38] in atom optics on a gas of sodium atoms by modulating a transverse external magnetic field and using a lock-in technique. Later, Crooker et al. [39] systematically investigated the spin noise in rubidium gas in a steady state experiment for a wide range of experimental conditions. For sufficient detuning from the probed optical resonance, off-resonant probing [40] even establishes a quantum non-demolition measurement of the atomic spin [41, 42] and represents a key ingredient of a series of light-matter and matter–matter entanglement experiments [43–45].

2.2 Spin noise in a nutshell In general, optical SNS measures the noise-power spectrum of the stochastically fluctuating spin polarization $s_z(t)$ projected onto the axis of light propagation, which is in the following defined by the z-axis. The Wiener–Chinchin theorem [46, 47] states that the autocorrelation function of the stochastic processes in the time domain is fully represented by the power-spectrum in the frequency domain. For example, the autocorrelation function of $s_z(t)$ with a characteristic homogenous spin decoherence rate $\gamma_s = 1/\tau_s$ can be written for $t > 0$ [18, 48, 49] as

$$s_z(t) = \langle s_z(0)s_z(t) \rangle \propto \cos(2\pi\nu_L t)e^{-\gamma_s t}. \tag{1}$$

Here, ν_L denotes the Larmor frequency in a potentially present transverse magnetic field. The power spectrum $S_{SN}(\nu)$ is obtained by taking the Fourier transformation (FFT) of $S_z(t)$ and results in

$$S_{SN}(\nu) = P_{SN}\left(\frac{\gamma_s}{\gamma_s^2 + \pi^2 4(\nu - \nu_L)^2} + \frac{\gamma_s}{\gamma_s^2 + \pi^2 4(\nu + \nu_L)^2}\right). \tag{2}$$

Here, $S_{SN}(\nu)$ consists of two mirrored Lorentzian functions each centered at $\pm\nu_L$. For frequencies $\nu_L > \gamma_s \gg 0$, the resulting noise spectra nicely follow a single Lorentz function where P_{SN} represents the integrated spin noise power. Care must be taken if the width of the Lorentz function strongly exceeds the Larmor frequency, i.e., $\gamma_s \gg \nu_L$. In this case, the measured line-shape of the spectrum changes since only positive frequencies are detected and the negative frequency range is folded back into the positive part of the frequency power spectrum.

Homogeneous spin decoherence processes generally result in a Lorentzian shaped spin noise contribution in the noise spectra with a full width at half maximum given by $\gamma_h = \gamma_s/\pi$. However, stochastic inhomogeneities in the sample broaden the spin noise signal due to, e.g., g-factor variations or hyperfine interaction and lead to a frequency spectrum generally following a normal distribution with a standard deviation σ_s. In this case, the pure inhomogeneous spin dephasing rate γ_i is given by $2\sigma_s = \gamma_i/\pi$ [19]. For the case that both – homogenous and inhomogeneous – processes contribute equally to the spin noise spectrum, a more detailed analysis based upon Voigt profiles is necessary (see also Ref. [50] for details).

Figure 1 depicts a standard experimental spin noise spectrum $S_{SN}(\nu)$ measured in n-doped bulk GaAs at cryogenic temperatures with an applied external transverse magnetic field of $B_{eff} = 30$ mT. The transverse magnetic field modulates the stochastic spin polarization with the respective Larmor frequency $\nu_L = g \times \mu_B |B_{eff}|/h$. A background spectrum acquired at much higher transverse magnetic fields has already been subtracted from the depicted spectrum, i.e., for the background spectrum all spin noise power has been shifted out of the detection range. The unit of measure for the noise power density in electrical engineering is $V^2 Hz^{-1}$, since it is standardized to the corresponding voltage dropping at a 50 Ω resistor. However, the Faraday rotation noise power $\langle \theta_F^2 \rangle$ is measured in radians (rad^2) and conversion for small rotation angles θ_F takes place by $P_{SN} = \langle \theta_F^2 \rangle (\alpha P_{laser})^2$, where α is the electro-optic gain of the detector and P_{laser} the probe laser power.

The integrated measured spin noise power P_{SN} is for small rotation angles proportional to the standard deviation

of the instantaneous polarization, which is calculated simply from binominal statistics for a fixed probability for each individual event. In the case of a single electron spin only two orientations $\pm 1/2$ are possible. Thus, the average mean deviation for a single spin from the zero average polarization is $\langle \sigma_{1/2}^2 \rangle = 1/4$. For an ergodic system, there is no difference if many measurements m are either taken in parallel or subsequently in time. In this case, the central limit theorem states that for large m the stochastics can be well described by a Gaussian probability distribution. Mathematically, for a given number of non-interacting electrons $N = N_\uparrow + N_\downarrow$ in thermal equilibrium the mean of each spin species $\uparrow(\downarrow)$ is thus $\langle N_{\uparrow(\downarrow)} \rangle = 0.5 N$ with a standard deviation of

$$\sigma_{\uparrow(\downarrow)} = (\langle N_{\uparrow(\downarrow)}^2 \rangle - \langle N_{\uparrow(\downarrow)} \rangle^2)^{1/2} = 0.5\sqrt{N}. \tag{3}$$

The average polarization $\langle (N_\uparrow - N_\downarrow)/(N_\uparrow + N_\downarrow) \rangle$ is zero in thermal equilibrium but the standard deviation of the Faraday rotation angle becomes

$$\langle \theta_F^2 \rangle^{1/2} \propto \frac{\sigma_\uparrow}{\langle N_\uparrow \rangle} + \frac{\sigma_\downarrow}{\langle N_\downarrow \rangle} = \sqrt{N}/N. \tag{4}$$

For a given bulk sample volume, which is determined by the sampling area A and the sampling length l, respectively, and a fixed carrier density $n = N/(Al)$ the spin noise power density S_{SN} increases with decreasing area A, i.e., with decreasing sampling focus. On the other hand, the spin noise power increases with the density n and length l. In the typical experimental setup, the length l is determined by the Rayleigh range of the focused light inside the sample whereat the optimal Rayleigh range is equal to the thickness of the sample. Please note that this relation holds only as long as a homogenous density of spins can be defined, i.e., for large m. The situation is especially different for single quantum dots, which have a much smaller effective volume than Al.

2.3 Technical implementation Figure 2 depicts the typical experimental cw-SNS setup: Linearly polarized probe light from a low noise and single mode laser source, e.g., from a stabilized diode laser, is transmitted through the sample and acquires a stochastic Faraday rotation angle $\theta_F(t)$. The fluctuating linear light polarization after traversing the sample is analyzed by a polarization bridge consisting of a polarizing beam splitter – which can be either a polarizing cube or a Wollaston prism – and a balanced photo receiver. The electrical output of the balanced receiver is amplified by an external low noise electrical amplifier and then further processed by spectral analysis.

The major noise source in optical SNS is in most cases optical photon shot noise, which strongly contributes to the total observed noise signal as a white background noise. The optical shot noise scales with the number of photons and is given by the laser light power P_{laser} and the photon energy E_{laser} with a frequency independent (white) noise power density $S_{WN} = 2\alpha^2 E_{laser} P_{laser}$ Electrical noise from the
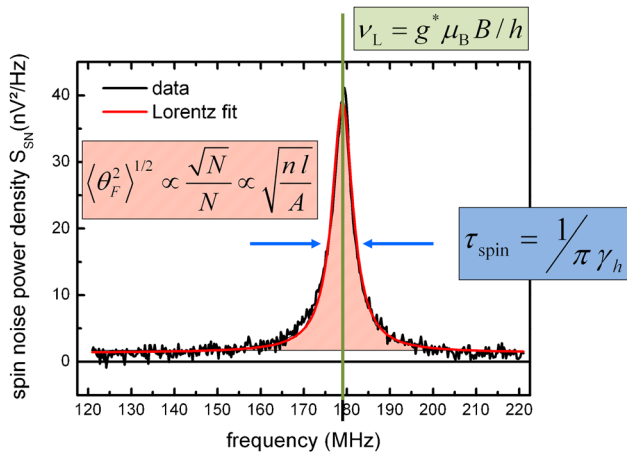

Figure 1 Typical experimental spin noise power density difference spectrum for a homogenous spin decay. The data has been recorded in n-type GaAs at low temperatures with an applied transverse magnetic field of 30 mT. The laser shot noise background has already been subtracted. The center frequency yields the Larmor frequency ν_L, the full-width at half maximum γ_h is a measure for the spin dephasing rate, and the integrated area depends *inter alia* on the square root of the number of contributing spins normalized by their total number.

Feature

Article

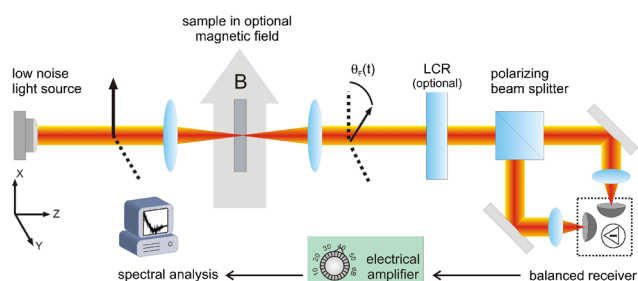Phys. Status Solidi B 251, No. 9 (2014)

1827

Figure 2 Standard setup for cw-semiconductor spin noise spectroscopy. A low noise light source provides linearly polarized light, which is transmitted through the sample. An optional magnetic field can modulate the stochastic spin polarization with a Larmor frequency or suppress the influence of, e.g., nuclear fields for certain geometries. The stochastic spin fluctuation is mapped onto the linear light polarization, which is then analyzed by a polarization bridge. An optional switchable polarization plate like a liquid-crystal retarder (LCR) or electro optic modulator can be used in order to suppress the Faraday rotation signal while leaving all other noise sources untouched. This enables an easy background acquisition if no magnetic field should be applied.

detector and amplifier further adds to the noise background and becomes significant at very low probe laser powers as they are for example used in single-spin noise spectroscopy [2, 51, 52]. The maximum height of the spin noise peak is $S_{SN}(\nu_L) = 2\langle\theta_F^2\rangle\gamma_s^{-1}(\alpha P_{laser})^2$ and depends strongly on the spin dephasing rate γ_s (cf. Eq. (2)), which makes the detection of short spin lifetimes more challenging in view of a constant background noise. For a given white background noise level S_{WN} and negligible other noise sources, the ratio η between peak spin noise density $S_{SN}(\nu_L)$ and S_{WN} decreases with increasing spin dephasing rate γ_s as $\eta = \langle\theta_F^2\rangle P_{laser}\gamma_s^{-1}/E_{laser}$ and ranges for typical semiconductor systems between 10^{-2} and 10^{-5} (see also Table 1 in Ref. [13]). However, some sample systems are inflicted with certain restrictions, which determine the maximal achievable value for η. For example, in some experimental implementations the probe light power has to be kept as small as possible in order to avoid residual absorption [2, 51, 52].

Recently Glasenapp et al. [53] investigate the possibilities to use a sophisticated way of polarimetry [54] in order to enhance the spin noise signal. They exploit the fact that the detected fluctuation amplitude increases linearly with increasing probe light power P_{laser} at the sample such that a higher probe light power in the actual experiment yields stronger signal. In order to keep the absolute light power on the two photo-diodes of the balanced detector limited they cross out most of the higher light power in one arm and attenuate the uncrossed arm with a neutral density filter. This straight-forward procedure leaves the Faraday noise fluctuation of the increased light power in principle untouched and at the same time still takes advantage of the balanced detection scheme to suppress all other common intensity fluctuations. In Ref. [53], Glasenapp et al. report a potential increase of several orders of magnitude in spin noise signal in n-GaAs, however, at the expense of an

increased spin dephasing rate due to the influence of higher probe light power. A similar way of taking advantage of this type of polarimetry is to enhance the sensitivity by detecting the Faraday rotation noise signal in the dark arm of a Mach–Zehnder interferometer like setup [55–57].

In addition, sophisticated polarimetry can be easily used to suppress the Faraday rotation signal without affecting the magnitude of the usually dominating photon shot noise by employing a switchable retardation waveplate in the detection setup (Fig. 2). This approach is very helpful if no magnetic field can be used to obtain a spectrum with an altered spin noise spectrum in order to produce an adequate difference spectrum, which contains spin noise only. This can be the case, if, for example, the magnetic field changes the shape of the spin noise or if the maximal available magnetic field strength is not strong enough to produce an adequate difference spectrum. A liquid crystal retarder (LCR) was successfully used in Ref. [58] for this purpose and Ref. [50] employed an electro-optic modulator (EOM) to switch between sensitivity on circular or linear birefringence, respectively. The EOM has the advantage, that it can be modulated much faster than the LCR, which reduces remaining experimental noise sources, which cannot be suppressed by the common noise rejection of the balanced detection setup.

2.4 Electrical spectral analysis A high efficiency in the spectral analysis is critical in order to obtain reliable spin noise spectra. The first SNS experiment on semiconductors was carried out by Oestreich et al. with an electrical sweeping spectrum analyzer resulting in a relatively low signal-to-noise ratio despite long integration times. Sweeping spectrum analyzers only sample one frequency window within the resolution bandwidth at a time. For example, a typical sweeping spectrum analyzer with a resolution bandwidth of 0.1 MHz scanning over a frequency window of 100 MHz uses only about 0.1% of the available information delivered by the detection setup. The introduction of real-time fast FFT spectrum analyzers into SNS in 2007 by Römer et al. [35] can be regarded as the starting shot of the current success of SNS in semiconductors. The tremendous advantage of real-time FFT spectral analysis is the high efficiency in time coverage of up to 100% due the potential seamless data acquisition of spin noise at all frequencies within the detection bandwidth. Typically, the acquired time data is divided into blocks with fixed size of a power of two and Fourier transformed in real time. Finally, the resulting Fourier power spectra are added up for averaging. The higher efficiency by more than 3 orders of magnitude allows even acquisition of spin noise spectra of n-GaAs in real-time and the higher sensitivity finally opened the way to the investigation of lower dimensional systems [59] and eventually to the optical detection of spin noise from a single spin, which is discussed further below.

2.5 Real-time FFT analysis Deeply connected with the real-time FFT analysis is the question of digitization of

the noise signals. In the case of cw-SNS, the bandwidth of the employed electrical analog-to-digital (A/D) conversion defines the upper limit on the detectable spin dephasing rates. Most SNS measurements have been restricted so far to sample systems, which show spin dephasing rates below 100 MHz, which can be digitized with a rather high accuracy [35, 58, 60–62]. Spin dephasing rates of a few 100 MHz have been demonstrated with 1-GHz digitizers [59] but faster digitizers are commercially available even up to bandwidths larger than 10 GHz. However, higher bandwidths are generally only available at the expense of a lower amplitude resolution given by the bit depth. At a first glance, this might pose an obstacle since small spin noise contributions are detected on a much larger shot noise background.

Müller et al. [63] performed realistic simulations of spin noise measurements in semiconductors in order to show to which extent a low bit depth of fast digitizers reduces the experimental sensitivity of SNS. The simulations are carried out assuming a low-signal strength η of the peak spin noise power in comparison to the photon shot noise density [13]. The low signal is typical for semiconductor systems in contrast to atomic gases due to the weaker effective coupling to the light field, i.e., the total oscillator strength of dense atomic gases is usually much higher compared to solid state systems. The ratio η has been kept fixed for the simulation ($\eta = 0.01$) since both, white and spin noise contributions, are equally amplified before being digitized. The A/D-conversion is characterized by the bit depth R and the sampling rate f_s of the digitizer [64], which determines the maximal detection bandwidth $B = f_s/2$ due to the Nyquist–Shannon theorem [65, 66]. Figure 3a schematically explains the quantization process of a continuous input x for an $R = 3$ bit digitizer. The quantized output y deviates from the analog input signal x by a quantization error $q = y - x$. If no overload occurs, i.e., $|x| > x_{max}$, and the quantization error

does not depend on x then q is approximately uniformly distributed over the maximal quantization error $2^{-R}/2$ with a standard deviation of $\sigma_q = 2^{-R}12^{-1/2}$ [67].

Figure 3b shows the signal-to-noise ratio SNR normalized by the number of averages N as a function of the input load σ_{WN} for different bit depths R. The maximum signal of $\eta = 0.01$ is well recovered for high bit depths. The rather weak dependence of the signal-to-noise ratio on the bit depth might seem unusual at first since the quantization error increases strongly with lower bit depth. Ironically, the continuously distributed white shot noise helps to save the SNR even for the lowest bit depths since the white noise serves efficiently as additive dither to the spin noise signal with amplitudes much smaller than the size of the least significant bit and heaves the spin noise signal above a certain detection threshold [69–72]. This explains as well the steep decrease in SNR for low overall input load at low bit depths in Fig. 3b. The simulations yield the best SNR for an optimal input load of $\sigma_{WN} = 0.1 \ldots 0.2$ V V depending on the bit depth for $x_{max} = 0.5$ V. At much higher input loads the overload error $\sigma_{q,over}$ adds to the total noise together with the white noise and quantization error and thereby reduces the SNR again. Müller et al. extracted the overload error from their simulations for an 8-bit quantizer, which is shown in Fig. 3b on the right axis.

A cost-effective way to implement the FFT analysis for very low frequencies in the kHz regime was shown by Schulte et al. [73]. Here, a standard sound card was used to study the spin dynamic of rubidium vapor in external magnetic fields on the order of a few μT. In this low frequency spin noise experiment, the high-resolution bit depth of the sound card of 24 bit made it possible to waive the usage of an additional voltage amplifier in order to obtain an optimized load of the digitizer. Together with the high signal strength in atomic gases this makes the setup described in Ref. [73] attractive for student laboratories.

3 Spin noise in semiconductors
3.1 Spin noise at different doping densities
One of the most intensively investigated material system in the research field of semiconductor spintronics is n-doped bulk GaAs since it is easily available with high quality and spin polarized electrons can be efficiently excited and detected optically due to the well-known selection rules. The most relevant spin relaxation mechanisms and experimental results in this material system are reviewed in Refs. [12, 31, 74]. Electron spin relaxation in n-doped GaAs is well understood for low temperatures and doping concentrations far above the metal-to-insulator transition (MIT) as well for all doping concentrations at high temperatures [75]. In these cases, the Dyakonov–Perel (DP) spin relaxation dominates since all electrons are delocalized and accordingly the spin relaxation times are short. On the other extreme of very low doping concentrations at low temperatures, the spin relaxation times are again rather short due to the distinct nature of the strong hyperfine interaction with the lattice nuclei [76–80]. In contrast, for doping concentrations at the
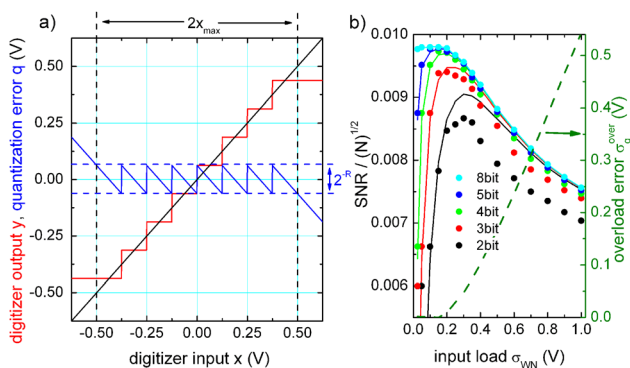
Figure 3 (a) Input (black)–output (red) characteristic (with quantization error (blue)) of a symmetric (with respect to zero) midrise 3-bit digitizer. (b) Signal-to-noise ratio SNR (left axis) normalized by the number of averages N [68] and the approximated overload error $\sigma_{q,over}$ as a function of the input load for different bit depths. The solid lines are calculated taking into account σ_q and $\sigma_{q,over}$. See also Ref. [63].

Phys. Status Solidi B 251, No. 9 (2014) 1829

Feature

Article

MIT and low temperatures, the spin relaxation times turn out to be very long. In this regime, the theoretical description becomes more complicated due to the intricate interplay of localized and free electrons. At the same time, the experiments become more difficult since optical excitation changes the carrier temperature and scattering times, which strongly affects the observed spin dynamic. Here, SNS provides a perfect experimental tool to unravel the undisturbed spin dynamic [81], i.e., the spin dynamic can be extracted without the traditional extrapolation to zero excitation power. Crooker et al. [36] and Römer et al. [61] complement the Hanle depolarization experiments performed by Dzhioev et al. [74] and measure the equilibrium spin relaxation time by SNS for different doping concentrations around the MIT over a wide temperature range.

Figure 4 shows the main results obtained by Römer et al. [61] for four different bulk n-GaAs samples with doping concentrations around the MIT $n_{MIT} \approx 1.8 \times 10^{16}$ cm^{-3} in dependence of the sample temperature. For very low doping densities ($n_d = 10^{14}$ cm^{-3}) and low temperatures, clearly the strong hyperfine interaction is responsible for the large spin dephasing rate. The strong localization is reduced for slightly higher doping densities of $n_d = 2.7 \times 10^{15}$ cm^{-3}, which in turn decreases the spin dephasing rate due to a more effective averaging over the random nuclear spin environment. At higher temperatures, the electrons delocalize easily into a Boltzmann distributed three-dimensional density-of-states. The spin dephasing rate now follows the typical $T^{3/2}$ dependence for the DP dominated regime. The same is true straightaway for the highest doping density of $n_d = 8.8 \times 10^{16}$ cm^{-3} (blue triangles in Fig. 4). However, for a doping density very close to the MIT ($n_d = 1.8 \times 10^{16}$ cm^{-3}), the spin dephasing time for this sample system becomes extremely long at low temperatures ($\tau_s \approx 270$ ns) due to the optimized interplay

between maximal averaging over the nuclear spin environment and minimized occupation of the spin split conduction band. The temperature dependence of the spin dephasing rate at the MIT regime consequently has to take into account both effects as is best described by a model considering spin dephasing in the hopping regime described by Shklovskii [82, 83] and anisotropic spin-exchange interaction in the realm of Dzyaloshinskii–Moriya mechanism [84, 85] put forward by Kavokin [86] and Putikka et al. [87]. More details are elucidated in Ref. [61].

The distinct dependence of the typical spin noise parameters like spin dephasing rate, integrated spin noise power and g-factor on the doping density n_d has been exploited in a proof of principle experiment for mapping the spatial distribution of n_d in all three dimensions by Römer et al. [58]. In this publication, the authors measured the doping density profile hidden *inside* a semiconductor stack as shown in Fig. 5. The key ingredient provided by SNS is that it (a) completely works in the transparent regime and (b) the main spin noise signal automatically originates from the focal volume due to the weighting by the inverse beam waist area as outlined above. This precursor experiment has been carried out with a limited detection bandwidth at low temperatures in order to avoid the strong increase in the spin dephasing rate with raising sample temperature [75]. However, the on-going development of SNS has overcome the bandwidth limitation put in place by electro-optic conversion and ultrafast SNS might yield a remedy in this field, which is discussed in more detail in the following section.

3.2 Ultrafast spin noise spectroscopy Fast dynamical spin processes in semiconductors and atomic gases under resonant excitation [88, 89] demand high detection bandwidths whereat the traditional electro-optical conversion in SNS dictates the technical limit of the maximum achievable time resolution. On the other hand, ultrafast laser spectroscopy provides a nearly unlimited time resolution what concerns spin coherence processes in semiconductors. Hence, an obvious way to extend the bandwidth of SNS is to merge the advantages of ultrafast laser spectroscopy with SNS. The usage of a single pulsed 80 MHz picosecond-laser oscillator has already enabled the extension of the detectable
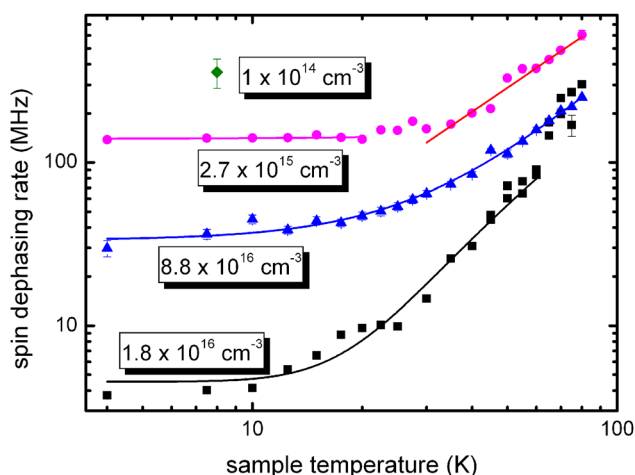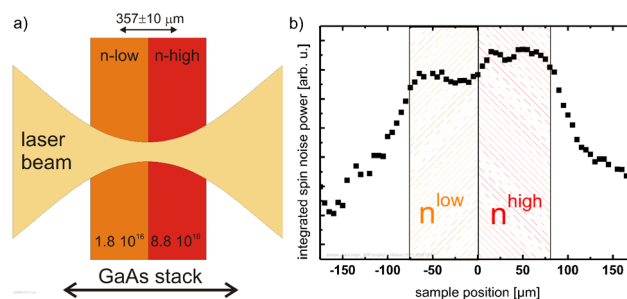
Figure 4 Spin dephasing rate for four different samples with doping concentrations around the metal-to-insulator transition (MIT) in dependence of the sample temperature measured by spin noise spectroscopy. The different models (solid lines) are described in the text. For details also see Ref. [61].

Figure 5 (a) Schematic setup of depth resolved spin noise spectroscopy (cf. Ref. [58]). (b) Integrated spin noise power in dependence of the axial probe focus position.

frequencies up to 16 GHz by stroboscopic undersampling of the spin dynamic into the accessible frequency regime [62]. Still, the complete full bandwidth of the electro-optical receivers dictates the upper limit of the detectable spin dephasing rates. In order to avoid this bottleneck, the spin correlation has to be probed completely by ultrafast pulses as suggested theoretically in Ref. [90]. Hübner et al. [91] merged SNS with scanning temporal ultrafast delay (STUD) techniques to overcome the bandwidth limitation. The recasted STUD-SNS method is perfectly tailored to capture the fast spin dynamic of systems, which are susceptible to direct optical excitation otherwise. The STUD-SNS setup is shown in Fig. 6 and consists of two free running picosecond laser oscillators, which differ in their repetition rate f_r by Δf and thereby automatically produce a pulse pair with a linearly oscillating delay Δt. This way, the pulse pairs subsequently probe the correlation of the spin dynamic without loss of information compared to cw-SNS under similar conditions [92]. The difference frequency Δf is typically set to a few kHz and thus the complete dynamic is recorded on a sub-millisecond timescale on the order of $1/\Delta f$, which directly entails the great advantage of inuring the technique against external instabilities. A further improvement of the signal-to-noise ratio can be achieved for spin coherence times τ_s on the order of $1/(4 f_r)$ since a background spectrum can be recorded in the same single scan. The optimal parameters for τ_s and Δf for this approach are calculated in Ref. [91]. The method of STUD-SNS is complementary to the ultrafast single laser SNS technique employed in Ref. [62], which has a potentially very high frequency resolution given by the number of points entering the FFT analysis but a limited bandwidth of $f_s/2$ set by the sampling frequency (see Section 2.5). On the other hand, STUD-SNS is resolution limited with a frequency resolution of $2 f_r$ but capable of detecting extremely high bandwidths given by the pulse width, e.g., $(100\,\mathrm{fs})^{-1} = 10\,\mathrm{THz}$.

A more optimized version of STUD-SNS for even shorter spin coherence times is employed by Berski et al. [50]. Here, the delay Δt is technically restricted to short times $\Delta t \lesssim 1\,\mathrm{ns}$ and controlled by a lock-to-clock system, which is advantageous for spin coherence times much shorter than the repetition period of the laser oscillators in order to obtain a high coverage of the acquisition time, which contains spin noise. The investigated model system is in this case highly doped n-GaAs with a well-known short spin lifetime on the order of a few hundred picoseconds. A typically measured ultrashort spin-correlation is shown as an inset in Fig. 6. In addition to the successful demonstration of ultrafast SNS with a full bandwidth of more than 60 GHz Berski et al. observe an inhomogeneous spin decoherence, which is attributed to the intrinsically present donor density fluctuation due to the growth of the host material at thermal equilibrium. Here, the spin of the individual electrons adding up to a statistically present spin polarization serves as a local probe of the three-dimensional environment inside the bulk material. A closely related effect was observed in a more advanced two-dimensional carrier system by Müller et al. [60], which is presented in the following section.

3.3 Quantum well systems The transition from bulk semiconductors to 2D systems has been a quite large transition for SNS since the absolute number of probed carriers reduces drastically from several billion to a few ten thousands. However, quantum wells bear the great advantage of engineering the relatively sharp optical transition energy according to the material systems at hand. Furthermore, the freedom of choice for certain symmetry constrains in the zinc-blende crystallographic system has been exploited [93] to obtain very long spin dephasing times in two-dimensional heterostructures with their quantization axis oriented in the (110)-direction. Henceforth, (110)-GaAs quantum wells attracted great attention in the realm of semiconductor spintronics since here the electron spin relaxation times are extremely long even at room temperature [94] and mostly limited by intersubband electron scattering induced spin relaxation (ISR) [95]. However, at low temperatures the impact of ISR is weak and without the DP mechanism [96] spin relaxation only takes place via the Bir–Aronov–Pikus mechanism resulting from electron–hole exchange interaction of free carriers [97, 98] or excitonic electron–hole spin interaction [99], which relevance increases with excitation densities [37]. SNS avoids optical excitation and is therefore perfectly suited to determine the experimentally unaltered contingently long intrinsic spin-relaxation time τ_z.

Müller et al. [60] demonstrated that the intrinsic, low temperature spin decoherence time τ_z in modulation n-doped GaAs (110) QWs can be measured by SNS and yields much longer τ_z than measured previously [94, 95]. In addition, the two-dimensional confinement bears the advantage to obtain a better understanding of the spatial electron dynamic. Here, Müller et al. [60] used the spin of the electron as a marking property to record the dynamic of electrons moving into and
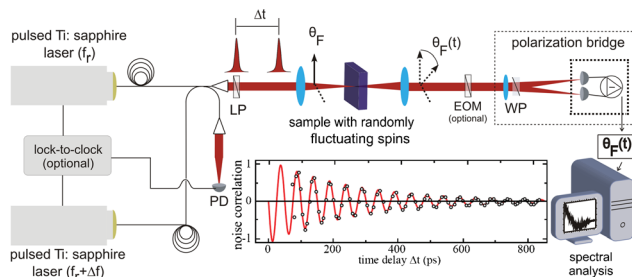

Figure 6 Schematic STUD-SNS setup (cf. Ref. [91]). Here, the time delay is provided automatically due to the difference Δf in the repetition rates of the laser oscillators. An extension of the setup is described in Ref. [50] where the time delay Δt is controlled by a lock-to-clock system and thus can be restricted to very short times. Here, an electro-optic modulator (EOM) helps to obtain a background spectrum similar to the liquid-crystal retarder described in Section 2.1. The inset shows a typical correlation function taken from Ref. [50].

Feature
_____
Article

Phys. Status Solidi B 251, No. 9 (2014)   1831

out-off the sampling area in the plane of the quantum well. The principle is shown in Fig. 7.

Figure 7a displays the characteristic scenario of the detected spin coherence and decoherence. The recorded spin dynamic is composed of at least two main components. One is the intrinsic spin decay rate γ_z^i while the other is determined by the probability of the electrons leaving the sampling area $A = \pi w_0^2$ due to a Brownian motion. The diffusion length for a classical Brownian motion is $2\sqrt{Dt}$ [3, 100] as shown in Fig. 7a, where D represents the spin diffusion length [101]. Figure 7b shows the measured spin decay rate of the stochastically oriented electron spins in dependence of the probe spot waist (radius) w_0 under different experimental conditions. It is clearly seen that for small sampling areas the spin dynamic is dominated by spin diffusion whereas for large areas the spin decay rate converges to its intrinsic value. The solid lines in Fig. 7b are a numerical calculation of the joint spin dynamic for different spin diffusion constants taking into account the Gaussian laser intensity distribution and an intrinsic spin decay rate of $\gamma_s^i = [23.9(1.4)\,\text{ns}]^{-1}$. Even though, yielding at that time one of the longest spin coherence times measured in (110)-GaAs quantum wells (see also Ref. [102]) there still seems to be an intrinsic limit. This limiting constraint has been identified to result from random Rashba fields originating from the internal electric fields on a mesoscopic scale due to fluctuating nature of dopant sheet densities for modulation doped quantum wells. These electric fields are the source for locally lifting the spin degeneracy in the (110)-direction [103–105]. This, however, brings the typical DP mechanism back into these promising two-dimensional systems. Griesbeck et al. [106] employed a specially designed (110)-grown heterostructure system in order to suppress the spin dephasing influence of random Rashba-fields and successfully obtained even longer spin dephasing times. The ultimate way to supress the influence of the band dispersion onto the spin dynamic are zero-dimensional semiconductor systems, which are discussed in the following section.
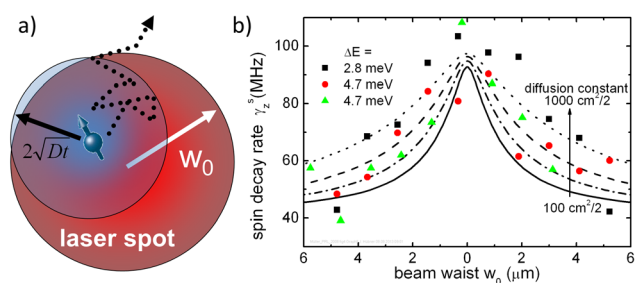
3.4 Spin noise in quantum dots In contrast to atoms, semiconductor quantum dots offer the unique property that the energy of the optical transitions can be engineered and single quantum dots can be selectively addressed. Furthermore, compared to higher dimensional semiconductor systems, all dispersion related spin dephasing mechanisms are much stronger suppressed in quantum dots. Therefore, the spins of carriers confined in quantum dots are favored as possible candidates for a quantum-bit implementation in solid state quantum information processing [107, 108]. The decoherence times of carrier spins in quantum dots are mainly limited by the strength of the hyperfine and dipole-like coupling to the nuclear spin bath [80] which is present in all typical III–V material based systems (cf. Table 1). An intelligent way to sidestep the influence of the hyperfine interaction is the investigation of the spin of holes which – unlike electrons – have p-type Bloch wave functions with a vanishing probability density at the nuclei [109–111]. Thus, instead of a strong Fermi-contact interaction hole-spins experience a potentially weaker dipole–dipole type coupling to the nuclear spin bath, which results in significantly longer spin relaxation times of holes compared to electrons. The remaining interaction magnitude is strain induced [112] due to mixing of the bands and could be even further reduced in GaAs quantum dots grown by droplet epitaxy [113]. Furthermore, the influence of the nuclear field can be quenched by an external longitudinal magnetic field, which exceeds the effective nuclear field [114, 115]. The hole-spin relaxation times are finally limited by single hole-acoustic-phonon scattering, which can produce a spin-flip between nuclear field induced Zeeman-split states, two-phonon processes [116] and quadrupolar coupling to local electrical fields [117]. Measurements on ensembles of self-assembled (InGa)As quantum dots already yielded hole spin lifetimes of a few ten nanoseconds measured by photoluminescence [114] and even longer for spin noise measurements [118]. On the downside, one quantum dot seldomly is alike another within an quantum dot ensemble. The obvious alternative is either implementing techniques to produce identical quantum dots or the investigation of individual quantum dots.

Dahbashi et al. [2] demonstrated in their recent paper, the first spin noise measurements on a single hole confined in an individual quantum dot enclosed in a Bragg-mirror cavity. The cavity enhances the Faraday rotation signal due to multiple passes of the electric field [119–121] and enables spin noise measurements in reflection geometry as sketched in Fig. 8a. Figure 8b shows the measured total spin noise power P_{SN} originating from an individual singly charged quantum dot (blue points, right axis) versus the detuning of the probe photon energy. The solid lines represent the spectral positions of the optical transitions of a charged (no $\pi_{x,y}$ splitting) and uncharged ($\pi_{x,y}$ splitting present) single quantum dot, respectively, measured by polarization resolved photoluminescence [122]. The charging state with an odd number of resident holes is identified by (a) the observation of a lacking splitting of the photoluminescence
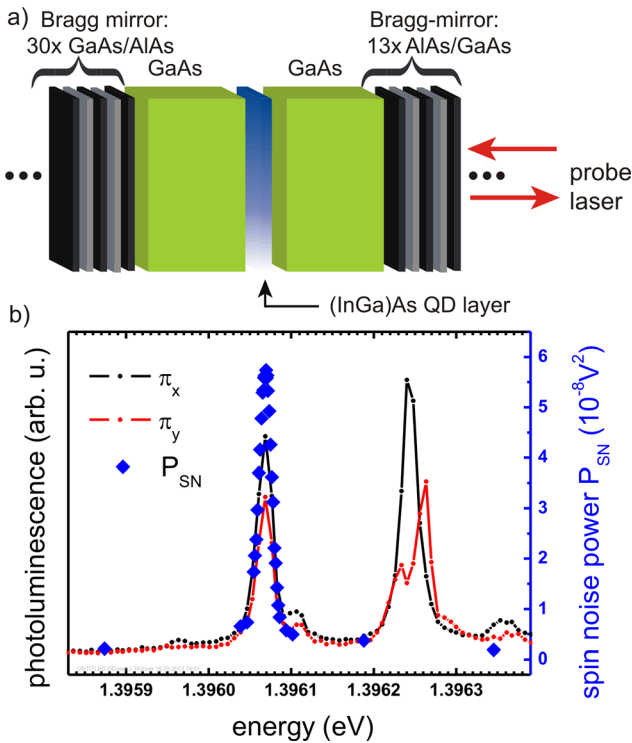

Figure 7 (a) Schematic representation of the spin diffusion leading to an effective spin decay rate detected in the sampling area given by the beam waist w_0. (b) Measured spin decay rate at a sample temperature of 20 K in dependence of the effective laser focus radius for different probing energies ΔE with respect to the electronic resonance. The solid lines represent the numerically calculated convolution of the joint intrinsic and diffusion limited spin decay. See also Ref. [60] for further details.

Figure 8 (a) Schematic representation of the investigated sample. One layer of self-assembled quantum dots is enclosed inside the electric field antinode of a semiconductor Bragg-mirror cavity. (b) Measured total spin noise power (blue points, right axis) versus detuning of the photon energy. The solid lines show the spectral positions of a charged (no $\pi_{x,y}$ splitting) and uncharged ($\pi_{x,y}$ splitting) quantum dot measured by photoluminescence. See also Ref. [2] for further details.

in the linear polarization basis $\pi_{x,y}$ and (b) by the p-type background doping, which has been measured before on the same sample even for a higher quantum dot density via the determination of a typical inhomogeneous hole-spin dephasing time [52].

Similar to recent spin noise measurements on ensembles of quantum dots [52, 59, 118] Dahbashi et al. [2] use a magnetic field to distinguish between the background noise and spin noise. Figure 9 schematically depicts the influence of an external magnetic field $\vec{B}_{ext}$ on the detected spin dynamic for an arbitrarily oriented spin $\vec{S}$ under the influence of a random nuclear field $\vec{B}_N$. The projection of $\vec{S}$ onto the effective magnetic field $\vec{B}_{eff}$ defines the two well-known transverse T_2-like (blue) and longitudinal T_1-like (red) spin dephasing and relaxation times, respectively. The temporal dynamic of the z-component of each component consequently appears either as a spin noise signal at the respective Larmor frequency $\nu_L = g^* \mu_B |B_{eff}|/h$ in the spin noise spectrum or around zero frequency, respectively. The temporal dynamic represented by the low frequency T_1-like contribution is determined by the timescale on which B_{eff} or B_N changes. In quantum dots, however, the change of B_N, e.g., due to nuclear spin diffusion can be very long,
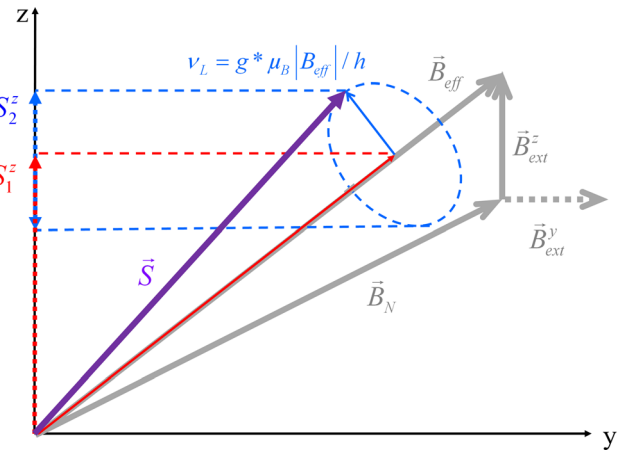

Figure 9 Schematic representation of the longitudinal (red) and transverse (blue) spin noise contributions for an arbitrary spin orientation $\vec{S}$. The random average nuclear field $\vec{B}_N$ adds up with an applied external longitudinal $\vec{B}_z$ or transversal field $\vec{B}_y$, respectively, to the effective local magnetic field acting upon the central electron or hole spin, respectively. For anisotropic transverse and axial g-factors with respect to the growth direction – as they are typical for self-assembled semiconductor quantum dots – the impact of the external magnetic field directions have to be scaled accordingly.

reaching timescale on the order of $\gg 1$s [123] but also depends on the intricate conditions of dynamic nuclear polarization if optical pumping is involved [124]. Without any external magnetic fields, B_{eff} is fully determined by the random nuclear field which magnitude follows a Maxwell-distribution for an average mean of $N \approx 10^5$ nuclear spins [77, 78, 125]. As a consequence, the detected spin noise spectrum related to the inhomogeneous transverse spin relaxation time T_2^* appears in the form of a Maxwell function which is usually much broader than the intrinsic decoherence time T_2. For an *equatorial* applied external magnetic field, i.e., perpendicular to the detection direction ($\vec{B}_y$ in Fig. 9) the respective spin noise spectrum appearing at the Larmor frequency transforms into a Gaussian distribution for $B_y \gg B_N$. However, for a large g-factor inhomogeneity – as typically colligated with quantum dot ensembles – the width of the Gaussian like noise power density increases linearly with B_y [19, 59]. The impact of oblique magnetic fields becomes even more complex if the effective g-factor g^* is strongly anisotropic with respect to the axial and equatorial directions [125]. For example, the anisotropy is very pronounced for hole spins in two- or lower dimensional systems due to their p-type nature of their waveforms [126]. But also electron spins are affected by g-factor anisotropies invoked by structural anisotropies [93].

External magnetic fields applied in the *axial* direction, i.e., the z-direction, evoke the opposite trend what concerns the appearance of nuclear field effects in the detected electron- or hole-spin dynamic. If B_z exceeds B_N, the distribution of B_{eff} strongly narrows, leaving effectively only the longitudinal S_1^z component. Please note, that the

Feature

Article

Phys. Status Solidi B 251, No. 9 (2014)
1833

distribution itself of B_N does not change under the condition $g_N \mu_N B \ll k_B T$, where g_N and μ_N are the nuclear g-factor and magneton, respectively, i.e., the nuclear spins are not polarized. Additionally, one has to keep in mind that the total spin noise power is constant in thermodynamic equilibrium, which entails that – if no polarization by the magnetic field takes place – the spin noise power from the suppressed inhomogeneous transverse contributions appears in the longitudinal contribution. Furthermore, under the condition $g^* \mu_B B \ll k_B T$, the measured spin longitudinal relaxation time merges with the transverse spin decoherence time $T_1 = T_2$ [15, 127] and the magnetic field has merely the task to suppress spin dephasing influence by the random nuclear fields. As a consequence, T_1 gives for low axial magnetic fields an approximate upper bound on the homogenous coherence time via the general relation $T_1 \geq T_2 \gg T_2^*$. The extracted coherence times of $\approx 180\,\mu s$ (Fig. 10) are therefore comparable to T_2 times extracted by Hahn-echo experiments for electrons in gate-defined quantum dots at ultralow temperatures [128].

Dahbashi et al. observed in their very recent spin noise measurements on single hole-spins a huge magnetic field dependence of T_1, i.e., an efficient suppression of B_N already for small magnetic fields of a few ten milli-Tesla. They finally reach measured hole-spin coherence times of $180\,\mu s$ for a magnetic field $B_z = 31\,mT$. The flat geometry of typical self-assembled quantum dots produces a strong g-factor anisotropy for holes, which is in favor of using small longitudinal magnetic fields in order to suppress the inhomogeneous spin dephasing by the random nuclear field (see also Ref. [125]). The extracted dependency of $\gamma_s \propto B^{-3/2}$ is not fully understood up to now and the experimental

findings might shed some light on the strongly discussed central-spin problem where the complex interaction of a central spin with a spin bath has produced theoretical predictions ranging from a strong increase of γ_s with B to exponential decrease of γ_s with B.

Besides the impact of the nuclear magnetic field onto the detected very long spin coherence times, residual absorption might reset the evolving spin coherence. In the case of the excitation of an additional electron–hole pair, the probability of the electron recombining with either of the holes forming a singlet is equal if one assumes a fast spin decoherence of the electron due to strong hyperfine interaction. In this case, excitation and reemission leaves behind a spin-up or spin-down state with 50% probability. The reset rate strongly depends on the detuning of the probe laser from the respective resonance and the photon flux, i.e., the probe light intensity. Interestingly, the relative detuning changes in this quantum dot sample during the measurement by a few μeV due to spectral wandering of the energetically narrow quantum dot resonance. These distinct and random shifts of the optical transitions are related to charge fluctuations of defects in the vicinity of the quantum dot and give rise to the inhomogeneous broadening of the integrated spin noise power P_{SN} shown in Fig. 8b). The distinct features of the Faraday rotation strength in dependence of detuning – as they are observed for homogenous atomic resonances – are in this sample hidden in the blend of the distinct single quantum dot environmental configurations. Nevertheless, the configurations are discrete which becomes obvious in the intensity dependence of the absorption-broadened spin decoherence rate shown in Fig. 10. The distinct configurations differ in their detuning with respect to the probe photon energy and alternate in their main contribution to the effective extracted width γ_h of the spin noise spectrum with increasing probe laser intensity. For three single quantum dot configurations with an intrinsic spin dephasing rate of $(7.6\,ms)^{-1}$ (dashed lines), the total calculated spin dephasing rate (solid line) nearly perfectly follows the measured data in dependency on the optical absorption rate given by the probe laser intensity (for details on the simulation and its parameters see Ref. [2]).
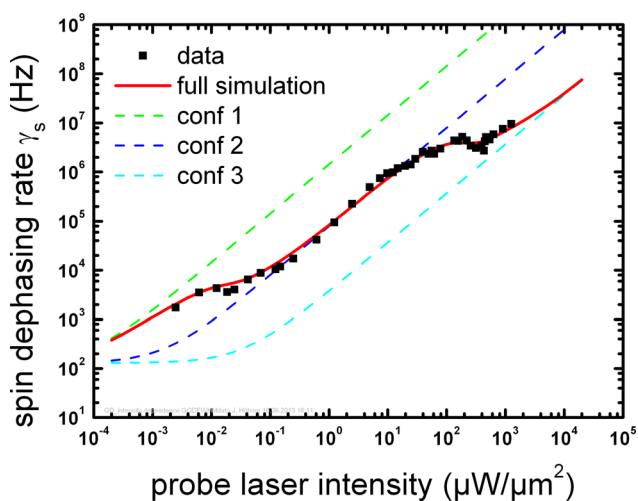
3.5 Spin noise in ZnO

Up to recently, all experiments on spin noise in semiconductors have been restricted to the typical III–V GaAs based semiconductor systems. However, there exists a vast number of experimental and theoretical works dealing with the specific peculiarities of the spin dynamic in II–VI semiconductors down to the single quantum dot level [129]. Especially oxide based II–VI wide band gap semiconductors like ZnO and ZnO/ZnMgO nanostructures have attracted high attention for their unique optoelectronic properties [130], potential application in semiconductor spintronics [11, 131–134], and spin based quantum-optronics [135]. ZnO promises very long electron spin coherence times even at room temperature, which results from the rather weak influence of the spin orbit splitting onto the conduction band states due to the large

Figure 10 Measured spin dephasing rate γ_s of a single heavy hole-spin confined in a self-assembled quantum dot in dependence of the probe-laser intensity (black squares). The red line is a simulation of the absorption induced shortening of the spin coherence taking into account the joint contribution of three different quantum dot resonances (dashed lines). The lowest measured value corresponds to $180\,\mu s$ while the model extrapolates a coherence time of $7.6\,ms$.

band gap and light atomic species [136, 137]. Furthermore, the scalability of hyperfine interaction in ZnO between lattice nuclei and confined carriers drawn from the cost-efficient availability of stable isotopes, which do not carry a nuclear spin [138] (see Table 1) makes this material very attractive concerning its applicability in semiconductor spintronics.

Horn et al. [139] investigate the intrinsic spin dynamic of donor bound electrons at the D^0X transition [140] in ZnO by optical SNS. The measurements reveal the transverse and longitudinal spin relaxation of donor bound electrons with respect to the mutual random hyperfine field whereat only a low fraction of the host nuclei carry a nuclear spin. Furthermore, they observe an additional, very short spin dephasing time, which is attributed to the increased interaction with defects located inside the effective donor volume. Figure 11 shows a set of spin noise measurements recorded for different transverse magnetic fields at low temperatures. The spin noise spectra consist of three major contributions which are the typical longitudinal T_1- and transverse T_2^*-like spin dephasing times and the T_2-like defect mediated spin decoherence time. The peculiar natural nuclear spin composition in ZnO yields an inhomogeneous spin lifetime of $T_2^* \approx 26$ ns for donor bound electrons, which is approximately an order of magnitude longer compare to the spin coherence time of donor bound electrons in GaAs.

4 Outlook SNS in semiconductors has proven itself as a very versatile and widely applicable tool for the low-invasive investigation of the spin dynamic in a variety of semiconductor systems. In addition to the persistent and high activity, both experimentally and theoretically, of employing SNS in classical [18, 88, 89, 141–144] and quantum atomic gases [145–147], there is a tremendously increasing interest
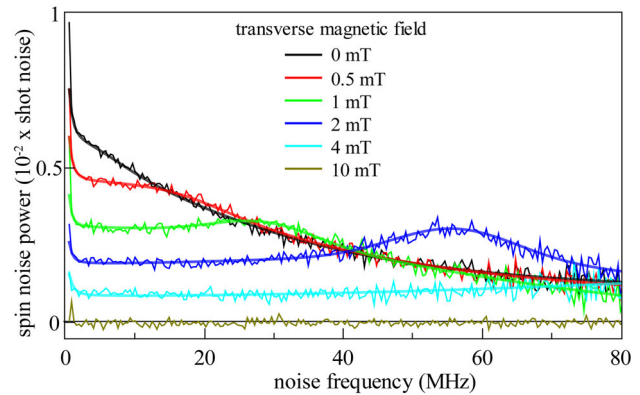

Figure 11 Spin noise spectra of bulk ZnO in units of optical shot noise power measured at different transverse magnetic fields. The background spectrum has been acquired at the maximum available field strength of $B_\perp = 10$ mT and subtracted, i.e., the shown spectrum at 10 mT represents the remaining uncertainty of two subsequent measurements. The solid lines represent fits with three different spin noise contributions, which are explained in the text. Further details on the sample and the experimental conditions are listed in Ref. [139].

of extending this technique even further into the field of semiconductor physics. Recent works investigate SNS in quantum wires [148–150] or spin noise of exciton polaritons in microcavities [151]. The intrinsic connection of the statistical temporal dynamic with the spectral composition of the associated noise spectrum even withstands deviation from thermodynamic equilibrium [152] as it is the case for quasi equilibrium conditions like the electrically driven spin Hall-effect [153]. Also semiconductor systems exist, which have comparable spectral properties and feature homogenous spin systems like atomic gases as, for example,

Table 1 Listing of the abundance of isotopes and their nuclear spin (shown in parentheses) for a selection of the most important semiconductor materials. The data is collected from the NIST isotope database.

compound	A-element	B-element
BN	^{10}B(3): 19.9%, ^{11}B(3/2): 80.1%	^{14}N(1): 99.6%, ^{15}N(1/2): 0.4%
AlP	^{27}Al(0): 100%	^{31}P(1/2): 100%
GaAs	^{69}Ga(3/2): 60.1%, ^{71}Ga(3/2): 39.9%	^{75}As(3/2): 100%
InSb	^{113}In(9/2): 4.3%, ^{115}In(9/2): 95.7%	^{121}Sb(5/2): 57.4%, ^{123}Sb(7/2): 42.6%%
C	^{12}C(0): 98.9%, ^{13}C(1/2): 1.1%	
Si	^{28}Si(0): 92.2%, ^{29}Si(1/2): 4.7%, ^{30}Si(0): 3.1%	
Ge	^{70}Ge(0): 21.2%, ^{72}Ge(0): 27.7%, ^{73}Ge(9/2): 7.7%, ^{74}Ge(0): 35.9%, ^{76}Ge(0): 7.4%	
BeO	^{9}Be(3/2): 100%	^{16}O(0): 99.8%, ^{17}O(5/2): 0.04%, ^{18}O(0): 0.2%
MgS	^{24}Mg(0): 79%, ^{25}Mg(5/2): 10%, ^{26}Mg(0): 11%	^{32}S(0): 95%, ^{33}S(3/2): 0.8%, ^{34}S(0): 4.2%, ^{36}S(0): 0.02%
ZnO	^{64}Zn(0): 48.6%, ^{66}Zn(0): 27.9%, ^{67}Zn(5/2): 4.1%, ^{68}Zn(0): 18.8%, ^{70}Zn(0): 0.6%	^{16}O(0): 99.8%, ^{17}O(5/2): 0.04%, ^{18}O(0): 0.2%
ZnSe	^{64}Zn(0): 48.6%, ^{66}Zn(0): 27.9%, ^{67}Zn(5/2): 4.1%, ^{68}Zn(0): 18.8%, ^{70}Zn(0): 0.6%	^{74}Se(0): 0.1%, ^{76}Se(0): 9.4%, ^{77}Se(0): 7.6%, ^{78}Se(0): 23.8%, ^{80}Se(0): 49.6%, ^{82}Se(0): 8.7%
CdTe	^{106}Cd(0): 1.3%, ^{108}Cd(0): 0.9%, ^{110}Cd(0): 12.5%, ^{111}Cd(1/2): 12.8%, ^{112}Cd(0): 23.1%, ^{113}Cd(1/2): 12.2%, ^{114}Cd(0): 28.7%	^{120}Te(0): 0.1%, ^{122}Te(0): 2.6%, ^{123}Te(1/2): 0.9%, ^{124}Te(0): 4.8%, ^{125}Te(1/2): 7.1%, ^{126}Te(0): 19%, ^{128}Te(0): 31.7%, ^{130}Te(0): 33.8%

Phys. Status Solidi B 251, No. 9 (2014)

Feature

Article

1835

localized donor (acceptor) bound carriers in very low doped ultrapure GaAs [154, 155] or isotopically pure silicon [156, 157]. The ability to detect ultra-long spin coherence times like in single quantum dots moves SNS one step closer to the realization of true quantum non-demolition measurements in semiconductors as they have already been successfully demonstrated in atom optics in a number of experiments [41, 145, 158, 159]. These promising preconditions might soon empower SNS in semiconductors to create quantum entanglement by the joint quantum non-demolition measurement of the linked entities as it was already successfully demonstrated in atom optics including the proof of entanglement of the spin degree of freedom in macroscopic atomic ensembles [43, 160]. Furthermore, the information obtained from spin noise is not limited to the three major entities elaborated in Section 2.1, i.e., the signal strength, the Larmor-frequency and spin dephasing rate corresponding to the 0th, 1st, and 2nd cumulant of a random variable, but is capable to provide a much deeper insight into correlated processes [161–163]. Such correlations obtained from the fluctuation spectrum of continuous weak measurements are envisioned to support the realization of quantum-bit operations with acceptable fidelities [164]. This applies, for example, to carrier spins confined in quantum dots [107, 165–169] with the prospect outlook to reach entanglement of the spin degree of freedom in quantum dots [170, 171], which can be possibly integrated into quantum-repeater schemes [172].

References

[1] M. Oestreich, M. Römer, R. J. Haug, and D. Hägele, Phys. Rev. Lett. **95**, 216603 (2005).
[2] R. Dahbashi, J. Hübner, F. Berski, K. Pierz, and M. Oestreich (2013), arXiv:1306.3183.
[3] A. Einstein, Ann. Phys. (Leipzig) **17**, 549 (1905).
[4] M. von Smoluchowski, Ann. Phys. **326**, 756 (1906).
[5] T. Boyer, Phys. Rev. D **11**, 790 (1975).
[6] A. de Oliveira-Costa, M. Tegmark, M. Zaldarriaga, and A. Hamilton, Phys. Rev. D **69**, 063516 (2004).
[7] R. H. Brown and R. Q. Twiss, Nature **177**, 27 (1956).
[8] R. Kubo, Rep. Prog. Phys. **29**, 255 (1966).
[9] S. A. Wolf, D. D. Awschalom, R. A. Buhrman, J. M. Daughton, S. von Molnár, M. L. Roukes, A. Y. Chtchelkanova, and D. M. Treger, Science **294**, 1488 (2001).
[10] M. Oestreich, J. Hübner, D. Hägele, M. Bender, N. Gerhardt, M. Hofmann, W. W. Rühle, H. Kalt, T. Hartmann, P. Klar, W. Heimbrodt, and W. Stolz, Adv. Solid State Phys. **41**, 173–186 (2001).
[11] I. Žutic, J. Fabian, and S. D. Sarma, Rev. Mod. Phys. **76**, 323 (2004).
[12] M. I. Dyakonov (ed.), Spin Physics in Semiconductors (Springer, Berlin, 2008).
[13] G. M. Müller, M. Oestreich, M. Römer, and J. Hübner, Physica E **43**, 569 (2010).
[14] V. S. Zapasskii, Adv. Opt. Photon. **5**, 131 (2013).
[15] F. Bloch, Phys. Rev. **70**, 460 (1946).
[16] N. Bloembergen, E. M. Purcell, and R. V. Pound, Phys. Rev. **73**, 679 (1948).
[17] I. Percival, Quantum State Diffusion (Cambridge University Press, Cambridge, 1998).
[18] G. E. Katsoprinakis, A. T. Dellis, and I. K. Kominis, Phys. Rev. A **75**, 042502 (2007).
[19] D. Pines and C. P. Slichter, Phys. Rev. **100**, 1014 (1955).
[20] T. Sleator, E. L. Hahn, C. Hilbert, and J. Clarke, Phys. Rev. Lett. **55**, 1742 (1985).
[21] M. Ocio, H. Bouchiat, and P. Monod, J. Phys. Lett. (France) **46**, 647 (1985).
[22] M. Alba, J. Hammann, M. Ocio, P. Refregier, and H. Bouchiat, J. Appl. Phys. **61**, 3683 (1987).
[23] W. Reim, R. H. Koch, A. P. Malozemoff, and M. B. Ketchen, Phys. Rev. Lett. **57**, 905 (1986).
[24] B. Stipe, H. Mamin, T. Stowe, T. Kenny, and D. Rugar, Phys. Rev. Lett. **86**, 2874 (2001).
[25] H. Mamin, R. Budakian, B. Chui, and D. Rugar, Phys. Rev. Lett. **91**, 207604 (2003).
[26] D. Rugar, R. Budakian, H. J. Mamin, and B. W. Chui, Nature **430**, 329 (2004).
[27] R. Budakian, H. J. Mamin, B. W. Chui, and D. Rugar, Science **307**, 408 (2005).
[28] H. Mamin, R. Budakian, B. Chui, and D. Rugar, Phys. Rev. B **72**, 024413 (2005).
[29] C. Degen, M. Poggio, H. Mamin, and D. Rugar, Phys. Rev. Lett. **99**, 250601 (2007).
[30] G. K. Woodgate, Elementary Atomic Structure, second ed. (Clarendon Press and Oxford University Press, Oxford and New York, 1980).
[31] F. Meier and B. P. Zakharchenya (eds.), Optical Orientation (North-Holland, Amsterdam, 1984).
[32] E. B. Aleksandrov and A. B. Mamyrin, JETP **45**, 247 (1977).
[33] D. H. McIntyre, C. E. Fairchild, J. Cooper, and R. Walser, Opt. Lett. **18**, 1816 (1993).
[34] T. Mitsui, Phys. Rev. Lett. **84**, 5292 (2000).
[35] M. Römer, J. Hübner, and M. Oestreich, Rev. Sci. Instrum. **78**, 103903 (2007).
[36] S. A. Crooker, L. Cheng, and D. L. Smith, Phys. Rev. B **79**, 035208 (2009).
[37] S. Oertel, S. Kunz, D. Schuh, W. Wegscheider, J. Hübner, and M. Oestreich, Europhys. Lett. **96**, 67010 (2011).
[38] E. B. Aleksandrov and V. S. Zapasskii, Sov. Phys. – JETP **54**, 64 (1981).
[39] S. A. Crooker, D. G. Rickel, A. V. Balatsky, and D. L. Smith, Nature **431**, 49 (2004).
[40] W. Happer and B. S. Mathur, Phys. Rev. Lett. **18**, 577 (1967).
[41] A. Kuzmich, N. P. Bigelow, and L. Mandel, Europhys. Lett. **42**, 481 (1998).
[42] A. Kuzmich, L. Mandel, J. Janis, Y. Young, R. Ejnisman, and N. Bigelow, Phys. Rev. A **60**, 2346 (1999).
[43] B. Julsgaard, A. Kozhekin, and E. S. Polzik, Nature **413**, 400 (2001).

[44] B. Julsgaard, J. Sherson, J. I. Cirac, J. Fiurášek, and E. S. Polzik, Nature **432**, 482 (2004).

[45] J. F. Sherson, H. Krauter, R. K. Olsson, B. Julsgaard, K. Hammerer, I. Cirac, and E. S. Polzik, Nature **443**, 557 (2006).

[46] N. Wiener, Acta Math. **55**, 117 (1930).

[47] A. Chintchin, Math. Ann. **109**, 604 (1934).

[48] M. Braun and J. König, Phys. Rev. B **75**, 085310 (2007).

[49] S. Kos, A. V. Balatsky, P. B. Littlewood, and D. L. Smith, Phys. Rev. B **81**, 064407 (2010).

[50] F. Berski, H. Kuhn, J. G. Lonnemann, J. Hübner, and M. Oestreich, Phys. Rev. Lett. **111**, 186602 (2013).

[51] J. Berezovsky, M. H. Mikkelsen, O. Gywat, N. G. Stoltz, L. A. Coldren, and D. D. Awschalom, Science **314**, 1916 (2006).

[52] R. Dahbashi, J. Hübner, F. Berski, J. Wiegand, X. Marie, K. Pierz, H. W. Schumacher, and M. Oestreich, Appl. Phys. Lett. **100**, 031906 (2012).

[53] P. Glasenapp, A. Greilich, I. I. Ryzhov, V. S. Zapasskii, D. R. Yakovlev, G. G. Kozlov, and M. Bayer, Phys. Rev. B **88**, 165314 (2013).

[54] V. S. Zapasskii, J. Appl. Spectrosc. **37**, 857 (1982).

[55] J. M. LaForge and G. M. Steeves, Appl. Phys. Lett. **91**, 121115 (2007).

[56] J. M. LaForge and G. M. Steeves, Rev. Sci. Instrum. **79**, 063106 (2008).

[57] J. Appel, P. J. Windpassinger, D. Oblak, U. B. Hoff, N. Kjærgaard, and E. S. Polzik, Proc. Natl. Acad. Sci. USA **106**, 10960 (2009).

[58] M. Römer, J. Hübner, and M. Oestreich, Appl. Phys. Lett. **94**, 112105 (2009).

[59] S. A. Crooker, J. Brandt, C. Sandfort, A. Greilich, D. R. Yakovlev, D. Reuter, A. D. Wieck, and M. Bayer, Phys. Rev. Lett. **104**, 036601 (2010).

[60] G. Müller, M. Römer, D. Schuh, W. Wegscheider, J. Hübner, and M. Oestreich, Phys. Rev. Lett. **101**, 206601 (2008).

[61] M. Römer, H. Bernien, G. Müller, D. Schuh, J. Hübner, and M. Oestreich, Phys. Rev. B **81**, 075216 (2010).

[62] G. M. Müller, M. Römer, J. Hübner, and M. Oestreich, Phys. Rev. B **81**, 121202(R) (2010).

[63] G. M. Müller, M. Römer, J. Hübner, and M. Oestreich, Appl. Phys. Lett. **97**, 192109 (2010).

[64] N. S. Jayant and P. Noll, Digital Coding of Waveforms: Principles and Applications To Speech and Video, Prentice-Hall Signal Processing Series (Prentice-Hall, Englewood Cliffs, NJ, 1984).

[65] H. Nyquist, Trans. Am. Inst. Electr. Eng. **47**, 617 (1928).

[66] C. Shannon, Proc. IRE **37**, 10 (1949).

[67] W. R. Bennett, Bell Syst. Tech. J. **27**, 446 (1948).

[68] The ordinate axis label in Fig. 2b in Ref. [63] is $SNR(N)^{1/2}$ such that the label in Fig. 3b changes accordingly to $SNR(N)^{1/2}$. The extracted results remain unaffected.

[69] L. Schuchman, IEEE Trans. Commun. **12**, 162 (1964).

[70] J. Vanderkooy and S. Lipshitz, J. Audio Eng. Soc. **32**, 106 (1984).

[71] R. Gray and T. Stockham, IEEE Trans. Inf. Theory **39**, 805 (1993).

[72] R. Wannamaker, S. Lipshitz, J. Vanderkooy, and J. Wright, IEEE Trans. Signal Process. **48**, 499 (2000).

[73] C. H. H. Schulte, G. M. Müller, H. Horn, J. Hübner, and M. Oestreich, Am. J. Phys. **80**, 240 (2012).

[74] R. I. Dzhioev, K. V. Kavokin, V. L. Korenev, M. V. Lazarev, B. Y. Meltser, M. N. Stepanova, B. P. Zakharchenya, D. Gammon, and D. S. Katzer, Phys. Rev. B **66**, 245204 (2002).

[75] S. Oertel, J. Hübner, and M. Oestreich, Appl. Phys. Lett. **93**, 132112 (2008).

[76] M. I. Dyakonov and V. I. Perel, Sov. Phys. – JETP **38**, 177 (1974).

[77] I. A. Merkulov, A. L. Efros, and M. Rosen, Phys. Rev. B **65**, 205309 (2002).

[78] A. Khaetskii, D. Loss, and L. Glazman, Phys. Rev. Lett. **88**, 186802 (2002).

[79] A. Faribault and D. Schuricht, Phys. Rev. B **88**, 085323 (2013).

[80] B. Urbaszek, X. Marie, T. Amand, O. Krebs, P. Voisin, P. Maletinsky, A. Högele, and A. Imamoglu, Rev. Mod. Phys. **85**, 79 (2013).

[81] Q. Huang, Phys. Rev. B **83**, 155204 (2011).

[82] B. I. Shklovskii, Phys. Rev. B **73**, 193201 (2006).

[83] K. V. Kavokin, Semicond. Sci. Technol. **23**, 114009 (2008).

[84] I. Dzyaloshinskii, J. Phys. Chem. Solids **4**, 241 (1958).

[85] T. Moriya, Phys. Rev. **120**, 91 (1960).

[86] K. V. Kavokin, Phys. Rev. B **64**, 075305 (2001).

[87] W. O. Putikka and R. Joynt, Phys. Rev. B **70**, 113201 (2004).

[88] H. Horn, G. M. Müller, E. M. Rasel, L. Santos, J. Hübner, and M. Oestreich, Phys. Rev. A **84**, 043851 (2011).

[89] W. Chalupczak and R. Godun, Phys. Rev. A **83**, 032512 (2011).

[90] S. Starosielec and D. Hägele, Appl. Phys. Lett. **93**, 051116 (2008).

[91] J. Hübner, J. G. Lonnemann, P. Zell, H. Kuhn, F. Berski, and M. Oestreich, Opt. Express **21**, 5872 (2013).

[92] This holds when both bandwidths are comparable and the laser repetition rate equals the cw-sampling rate. Accordingly, the total detected spin noise power is the same for identical average probe photon fluences.

[93] J. Hübner, S. Kunz, S. Oertel, D. Schuh, M. Pochwaa, H. Duc, J. Förstner, T. Meier, and M. Oestreich, Phys. Rev. B **84**, 041301(R) (2011).

[94] Y. Ohno, R. Terauchi, T. Adachi, F. Matsukura, and H. Ohno, Phys. Rev. Lett. **83**, 4196 (1999).

[95] S. Döhrmann, D. Hägele, J. Rudolph, M. Bichler, D. Schuh, and M. Oestreich, Phys. Rev. Lett. **93**, 147405 (2004).

[96] M. I. Dyakonov and V. I. Perel, Sov. Phys. – Solid State **13**, 3023 (1972).

[97] G. L. Bir, A. G. Aronov, and G. E. Pikus, Sov. Phys. – JETP **42**, 705 (1976).

[98] J. Zhou and M. W. Wu, Phys. Rev. B **77**, 075318 (2008).

[99] M. Z. Maialle, E. A. de Andrada e Silva, and L. J. Sham, Phys. Rev. B **47**, 15776 (1993).

[100] G. Bergmann, Phys. Rev. B **28**, 2914 (1983).

[101] C. P. Weber, N. Gedik, J. E. Moore, J. Orenstein, J. Stephens, and D. D. Awschalom, Nature **437**, 1330 (2005).

[102] J. O. D. D. Couto, F. Iikawa, J. Rudolph, R. Hey, and P. V. Santos, Phys. Rev. Lett. **98**, 036603 (2007).

[103] M. M. Glazov, M. A. Semina, and E. Y. Sherman, Phys. Rev. B **81**, 115332 (2010).

[104] M. Glazov, E. Sherman, and V. Dugaev, Physica E **42**, 2157 (2010).

[105] Y. Zhou and M. W. Wu, Europhys. Lett. **89**, 57001 (2010).

Phys. Status Solidi B 251, No. 9 (2014)

Feature
Article

1837

[106] M. Griesbeck, M. Glazov, E. Sherman, D. Schuh, W. Wegscheider, C. Schüller, and T. Korn, Phys. Rev. B **85**, 085313 (2012).

[107] D. Loss and D. P. DiVincenzo, Phys. Rev. A **57**, 120 (1998).

[108] Y. Yamamoto, Jpn. J. Appl. Phys. **50**, 100001 (2011).

[109] E. I. Gryncharova and V. I. Perel, Sov. Phys. – Semicond. **11**, 997 (1977).

[110] D. Brunner, B. D. Gerardot, P. A. Dalgarno, G. Wust, K. Karrai, N. G. Stoltz, P. M. Petroff, and R. J. Warburton, Science **325**, 70 (2009).

[111] E. A. Chekhovich, M. M. Glazov, A. B. Krysa, M. Hopkinson, P. Senellart, A. Lemaître, M. S. Skolnick, and A. I. Tartakovskii, Nature Phys. **9**, 74 (2012).

[112] F. Maier and D. Loss, Phys. Rev. B **85**, 195323 (2012).

[113] T. Amand, B. Urbaszek, G. Sallen, S. Kunz, T. Kuroda, T. Belhadj, A. Kunold, T. Mano, M. Abbarchi, D. Lagarde, X. Marie, K. Sakoda, H.-J. M. Drouhin, J.-E. Wegrowe, and M. Razeghi, Proc. SPIE **81000**, 81000H (2011).

[114] B. Eble, C. Testelin, P. Desfonds, F. Bernardot, A. Balocchi, T. Amand, A. Miard, A. Lemaitre, X. Marie, and M. Chamarro, Phys. Rev. Lett. **102**, 146601 (2009).

[115] P. Fallahi, S. T. Ylmaz, and A. Imamoglu, Phys. Rev. Lett. **105**, 257402 (2010).

[116] J. Fischer, W. Coish, D. Bulaev, and D. Loss, Phys. Rev. B **78**, 155329 (2008).

[117] N. A. Sinitsyn, Y. Li, S. A. Crooker, A. Saxena, and D. L. Smith, Phys. Rev. Lett. **109**, 166605 (2012).

[118] Y. Li, N. Sinitsyn, D. L. Smith, D. Reuter, A. D. Wieck, D. R. Yakovlev, M. Bayer, and S. A. Crooker, Phys. Rev. Lett. **108**, 186603 (2012).

[119] A. Kavokin, M. Vladimirova, M. Kaliteevski, O. Lyngnes, J. Berger, H. Gibbs, and G. Khitrova, Phys. Rev. B **56**, 1087 (1997).

[120] Y. Q. Li, D. W. Steuerman, J. Berezovsky, D. S. Seferos, G. C. Bazan, and D. D. Awschalom, Appl. Phys. Lett. **88**, 193126 (2006).

[121] R. Giri, S. Cronenberger, M. Vladimirova, D. Scalbert, K. V. Kavokin, M. M. Glazov, M. Nawrocki, A. Lemaître, and J. Bloch, Phys. Rev. B **85**, 195313 (2012).

[122] M. Bayer, G. Ortner, O. Stern, A. Kuther, A. Gorbunov, A. Forchel, P. Hawrylak, S. Fafard, K. Hinzer, T. Reinecke, S. Walck, J. Reithmaier, F. Klopf, and F. Schäfer, Phys. Rev. B **65**, 195315 (2002).

[123] A. Nikolaenko, E. Chekhovich, M. Makhonin, I. Drouzas, A. Van'kov, J. Skiba-Szymanska, M. Skolnick, P. Senellart, D. Martrou, A. Lemaître, and A. Tartakovskii, Phys. Rev. B **79**, 081303(R) (2009).

[124] V. K. Kalevic, K. V. Kavokin, and I. A. Merkulov, in: Spin physics in semiconductors, Springer Series in Solid-State Sciences, Vol. 157, edited by M. I. Dyakonov (Springer, Berlin, 2008), pp. 309–346.

[125] M. Glazov and E. Ivchenko, Phys. Rev. B **86**, 115308 (2012).

[126] R. Winkler, Spin–Orbit Coupling Effects in Two-Dimensional Electron and Hole Systems, Springer Tracts in Modern Physics, Vol. 191 (Springer, Berlin/Heidelberg, 2003).

[127] H. Torrey, Phys. Rev. **104**, 563 (1956).

[128] H. Bluhm, S. Foletti, I. Neder, M. Rudner, D. Mahalu, V. Umansky, and A. Yacoby, Nature Phys. **7**, 109 (2011).

[129] C. L. Gall, A. Brunetti, H. Boukari, and L. Besombes, Phys. Rev. B **85**, 195312 (2012).

[130] Ü. Özgür, J. Appl. Phys. **98**, 041301 (2005).

[131] T. Dietl, H. Ohno, F. Matsukura, J. Cibert, and D. Ferrand, Science **287**, 1019 (2000).

[132] S. Ghosh, D. W. Steuerman, B. Maertz, K. Ohtani, H. Xu, H. Ohno, and D. D. Awschalom, Appl. Phys. Lett. **92**, 162109 (2008).

[133] D. Lagarde, A. Balocchi, P. Renucci, H. Carrère, F. Zhao, T. Amand, X. Marie, Z. X. Mei, X. L. Du, and Q. K. Xue, Phys. Rev. B **78**, 033203 (2008).

[134] N. Janßen, K. M. Whitaker, D. R. Gamelin, and R. Bratschitsch, Nano Lett. **8**, 1991 (2008).

[135] W. K. Liu, K. M. Whitaker, A. L. Smith, K. R. Kittilstved, B. H. Robinson, and D. R. Gamelin, Phys. Rev. Lett. **98**, 186804 (2007).

[136] S. Ghosh, V. Sih, W. H. Lau, D. D. Awschalom, S.-Y. Bae, S. Wang, S. Vaidya, and G. Chapline, Appl. Phys. Lett. **86**, 232507 (2005).

[137] N. Harmon, W. Putikka, and R. Joynt, Phys. Rev. B **79**, 115204 (2009).

[138] K. M. Whitaker, S. T. Ochsenbein, A. L. Smith, D. C. Echodu, B. H. Robinson, and D. R. Gamelin, J. Phys. Chem. C **114**, 14467 (2010).

[139] H. Horn, A. Balocchi, X. Marie, A. Bakin, A. Waag, M. Oestreich, and J. Hübner, Phys. Rev. B **87**, 045312 (2013).

[140] C. F. Klingshirn, A. Waag, A. Hoffmann, and J. Geurts, Zinc Oxide: From Fundamental Properties Towards Novel Applications (Springer, Heidelberg/London, 2010).

[141] B. Mihaila, S. A. Crooker, D. Rickel, K. Blagoev, P. Littlewood, and D. Smith, Phys. Rev. A **74**, 043819 (2006).

[142] I. Kominis, Phys. Rev. Lett. **100**, 073002 (2008).

[143] G. E. Katsoprinakis, M. Polis, A. Tavernarakis, A. T. Dellis, and I. K. Kominis, Phys. Rev. A **77**, 054101 (2008).

[144] V. S. Zapasskii, A. Greilich, S. A. Crooker, Y. Li, G. G. Kozlov, D. R. Yakovlev, D. Reuter, A. D. Wieck, and M. Bayer, Phys. Rev. Lett. **110**, 176601 (2013).

[145] J. Sørensen, J. Hald, and E. Polzik, Phys. Rev. Lett. **80**, 3487 (1998).

[146] B. Mihaila, S. A. Crooker, K. Blagoev, D. Rickel, P. Littlewood, and D. Smith, Phys. Rev. A **74**, 063608 (2006).

[147] G. Bruun, B. Andersen, E. Demler, and A. Sørensen, Phys. Rev. Lett. **102**, 030401 (2009).

[148] M. M. Glazov and E. Y. Sherman, Phys. Rev. Lett. **107**, 156602 (2011).

[149] P. Agnihotri and S. Bandyopadhyay, J. Phys.: Condens. Matter **24**, 215302 (2012).

[150] P. Peddibhotla, F. Xue, H. I. T. Hauge, S. Assali, E. P. A. M. Bakkers, and M. Poggio, Nature Phys. **9**, 631 (2013).

[151] M. M. Glazov, M. A. Semina, E. Y. Sherman, and A. V. Kavokin, Phys. Rev. B **88**, 041309(R) (2013).

[152] F. Li, Y. V. Pershin, V. A. Slipko, and N. A. Sinitsyn, Phys. Rev. Lett. **111**, 067201 (2013).

[153] V. A. Slipko, N. A. Sinitsyn, Y. V. Pershin, Phys. Rev. B **88**, 20 (2013).

[154] C. H. van der Wal and M. Sladkov, Solid State Sci. **11**, 935 (2009).

[155] M. Sladkov, A. U. Chaubal, M. P. Bakker, A. R. Onur, D. Reuter, A. D. Wieck, and C. H. van der Wal, Phys. Rev. B **82**, 121308 (2010).

[156] J. J. L. Morton A. M. Tyryshkin, R. M. Brown, S. Shankar, B. W. Lovett, A. Ardavan, E. E. Haller, J. W. Ager, and S. A. Lyon, Nature **455**, 1085 (2008).

[157] S. Simmons, R. M. Brown, H. Riemann, N. V. Abrosimov, P. Becker, H.-J. Pohl, M. L. W. Thewalt, K. M. Itoh, and J. J. L. Morton, Nature **470**, 69 (2011).

[158] J. M. Geremia, J. Stockton, and H. Mabuchi, Phys. Rev. Lett. **94**, 203002 (2005).

[159] V. Shah, G. Vasilakis, and M. V. Romalis, Phys. Rev. Lett. **104**, 013601 (2010).

[160] J. Hald, J. L. Sørensen, C. Schori, and E. S. Polzik, Phys. Rev. Lett. **83**, 1319 (1999).

[161] S. Starosielec, R. Fainblat, J. Rudolph, and D. Hägele, Rev. Sci. Instrum. **81**, 125101 (2010).

[162] Y. V. Pershin, V. A. Slipko, D. Roy, and N. A. Sinitsyn, Appl. Phys. Lett. **102**, 202405 (2013).

[163] R.-B. Liu, S.-H. Fung, H.-K. Fung, A. N. Korotkov, and L. J. Sham, New J. Phys. **12**, 013018 (2010).

[164] T. Fink and H. Bluhm, Phys. Rev. Lett. **110**, 010403 (2013).

[165] J. R. Petta, Science **309**, 2180 (2005).

[166] T. M. Godden, J. H. Quilter, A. J. Ramsay, Y. Wu, P. Brereton, S. J. Boyle, I. J. Luxmoore, J. Puebla-Nunez, A. M. Fox, and M. S. Skolnick, Phys. Rev. Lett. **108**, 017402 (2012).

[167] T. Godden, J. Quilter, A. Ramsay, Y. Wu, P. Brereton, I. Luxmoore, J. Puebla, A. Fox, M. Skolnick, T. M. Godden, J. H. Quilter, A. J. Ramsay, I. J. Luxmoore, A. M. Fox, and M. S. Skolnick, Phys. Rev. B **85**, 155310 (2012).

[168] D. Roy, Y. Li, A. Greilich, Y. V. Pershin, A. Saxena, and N. A. Sinitsyn, Phys. Rev. B **88**, 045320 (2013).

[169] A. V. Kuhlmann, J. Houel, A. Ludwig, L. Greuter, D. Reuter, A. D. Wieck, M. Poggio, and R. J. Warburton, Nature Phys. **9**, 570 (2013).

[170] C. Y. Hu, A. Young, J. L. O'Brien, W. J. Munro, and J. G. Rarity, Phys. Rev. B **78**, 085307 (2008).

[171] J. Chen, T. Cubitt, A. Harrow, and G. Smith, Phys. Rev. Lett. **107**, 250504 (2011).

[172] T.-J. Wang, S.-Y. Song, and G. L. Long, Phys. Rev. A **85**, 062311 (2012).